1 **Table of contents**

3 **Text S1.** Sampling of aerosol filters.

4 **Text S2.** Additional setting information on the box model simulation of 28 September

5 2021.

6 **Text S3.** The determination of $J_{NO_3^-(aq)}$ and $J_{O_3 \rightarrow O^1D}$ in the chamber and ambient air.

7 **Text S4.** Additional laboratory experiments.

9 **Figure S1.** The location of the observation site, Cape D'Aguilar.

10 **Figure S2.** The variation of HCOOH sensitivity with RH.

11 **Figure S3.** The 24-h backward trajectories of different kinds of air masses during the

12 field campaign.

13 **Figure S4.** The schematic diagram of the photochemical aging experiment.

14 **Figure S5.** The sources of CH_2OO in the modified case on 28 September 2021.

15 **Figure S6.** The model results on 28 October 2021.

16 **Figure S7.** Additional laboratory experiments show that HCOOH was produced by

17 nitrate rather than HONO.

18

19 **Table S1.** The instruments and measured species or parameters in the field campaign.

20 **Table S2.** Summary of the $PM_{2.5}$ sampling information.

21 **Table S3.** Input parameters to the box model of 28 September 2021.

22

Text S1. Sampling of aerosol filters.

We collected ambient aerosols at Cape D'Aguilar Super Site in Autumn for photochemical aging experiments. The $PM_{2.5}$ samples were collected on quartz-fiber filters (8×10 inches) using a PUF-1000 high-volume sampler with a flow rate of 999 Lpm in 2020. All samplings were performed from 11:00 am local time (LT) to 10:00 am LT of the next day. The filters were pre-fired at 900 ℃ for 4 hours to remove organic artifacts and stored in a freezer at -20 ℃. Fractions with a given surface area from one randomized-chosen filter were used to perform the photochemical experiments or other analyses.

Text S2. Additional setting information on the box model simulation of 28 September 2021.

The observation data on 28 September was used as input to constrain the model with a time step of 5 min (Table S3). The data of trace gases (including O_3, NO, NO_2, CO and SO_2) and data obtained by ToF-CIMS (including HONO and N_2O_5) were averaged to 5-min resolution. For the VOCs and OVOCs species, linear interpolations were applied. The variables "ModelOptions.EndPointsOnly" and "ModelOptions.LinkSteps" were set to "1". The variable "ModelOptions.IntTime" was set to "300". No family conservation was used. Readers are referred to a F0AM description paper for more information (Wolfe et al., 2016).

Text S3. The determination of $J_{NO_3^-(aq)}$ and $J_{O_3 \rightarrow O^1D}$ in the chamber and ambient air.

The $J_{NO_3^-(aq)}$ and $J_{O_3 \rightarrow O^1D}$ in the chamber was calculated by (Eq. (1)),

$$J = \int q(\lambda)\sigma(\lambda)I(\lambda)d\lambda \qquad (1)$$

where $q(\lambda)$ is the quantum yield at wavelength λ (nm); $\sigma(\lambda)$ is the cross-section at wavelength λ; $I(\lambda)$ is the flux of xenon lamp at wavelength λ and was calculated by converting the irradiation energy spectra of the lamp (Fig. 6d) to photon flux based on Planck's equation. The $q(\lambda)$ and $\sigma(\lambda)$ of aqueous nitrate at 298 K were derived from (Chu & Anastasio, 2003). The $q(\lambda)$ and $\sigma(\lambda)$ of O_3 generating O^1D were adopted from the recommended value from IUPAC under 298 K (https://uv-vis-spectral-atlas-mainz.org/uvvis/index.html). The $J_{NO_3^-(aq)}$ and $J_{O_3 \rightarrow O^1D}$ in the ambient was calculated by the Tropospheric Ultraviolet and Visible (TUV) radiation model (https://www.acom.ucar.edu/Models/TUV/Interactive_TUV/) under clear sky conditions and then scaled to the field-measured jNO_2.

Text S4. Additional laboratory experiments.

Since HONO and HCOOH were simultaneously observed during the photochemical aging process, it is possible that HCOOH was produced from the heterogeneous

61   reactions between gas-phase OH radicals and particles. To check this possibility, an
62   experiment was conducted as follows (Fig. S7). 4 Lpm HONO-containing air (78% RH,
63   7.2 ppb HONO, balanced with zero air) was injected into the chamber. The solution
64   was prepared with 0.15 wt.% HCHO but without adding $NaNO_3$. The pH of the solution
65   was also adjusted to 2.7 using sulfuric acid. The background HCOOH concentration
66   was determined as 308.9 ppt when illuminating the chamber without the solution. After
67   adding the solution, the HCOOH concentration increased to 428.8 ppt. After
68   normalizing the HONO concentration in this experiment to that in the previous solution
69   experiments containing $NaNO_3$ (0.77 ppb HONO, 0.62 ppb HCOOH) (Fig. 6c), the
70   increased HCOOH concentration is 12.8 ppt, which is negligible. The conclusion is the
71   same when compared with the filter irradiation experiments (4.1 ppb HONO, 5.6 ppb
72   HCOOH). Therefore, the HONO photolysis contributes little to HCOOH production.
73

74 **Supplementary figures**
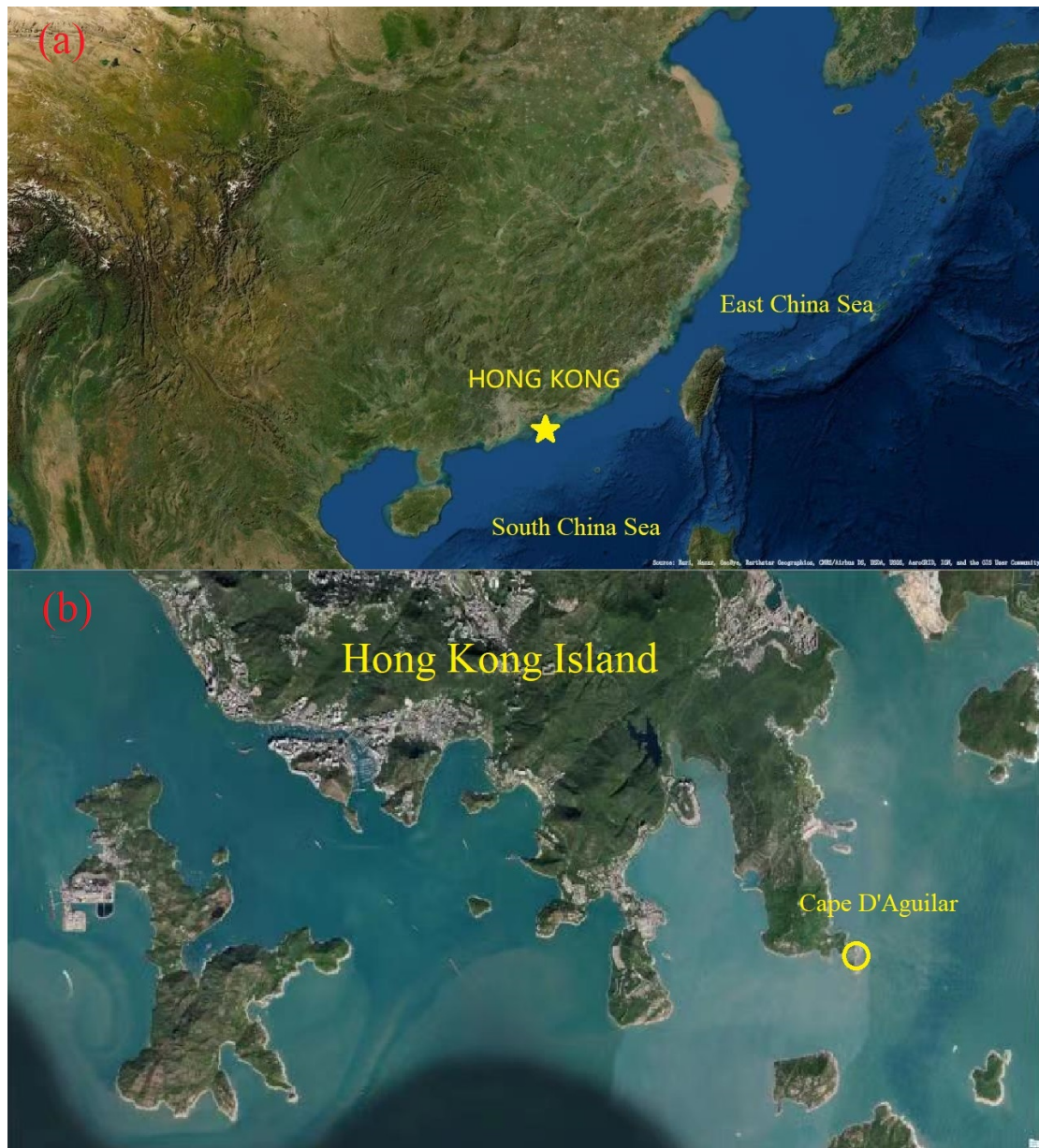
75

76 **Figure S1.** The location of the observation site, Cape D'Aguilar. (a) The location of
77 Hong Kong in South China. (b) The field observation site in Hong Kong Island. The
78 source is from Esri, Maxar, GeoEye, Earthstar Geographics, CNES/Airbus DS, USDA,
79 USGS, AeroGRID, IGN, and the GIS User Community.
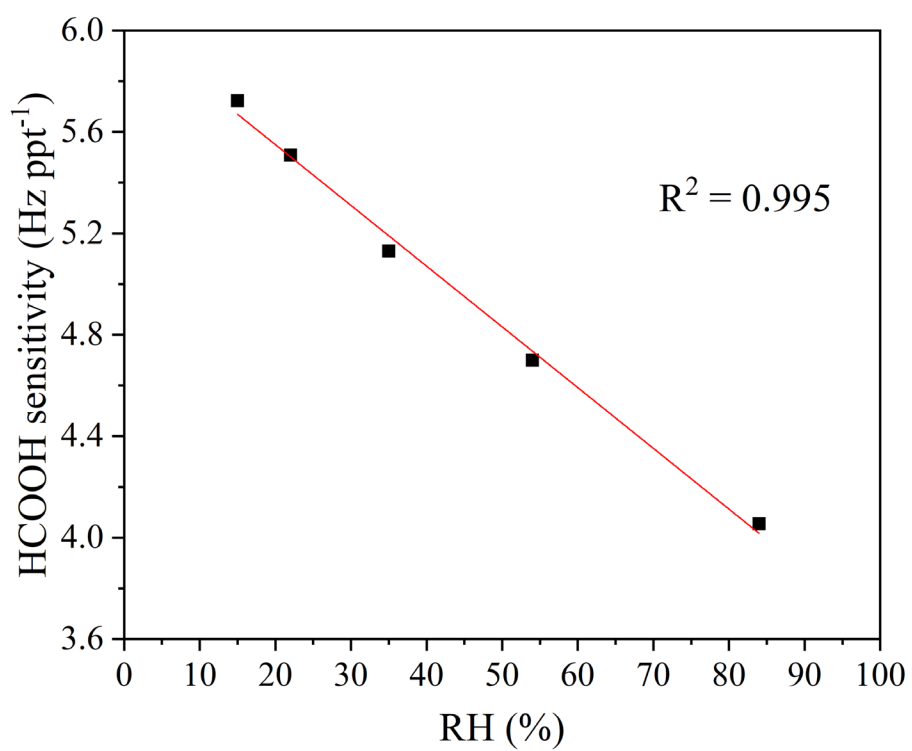
80

81   **Figure S2.** The variation of HCOOH sensitivity with RH.

82
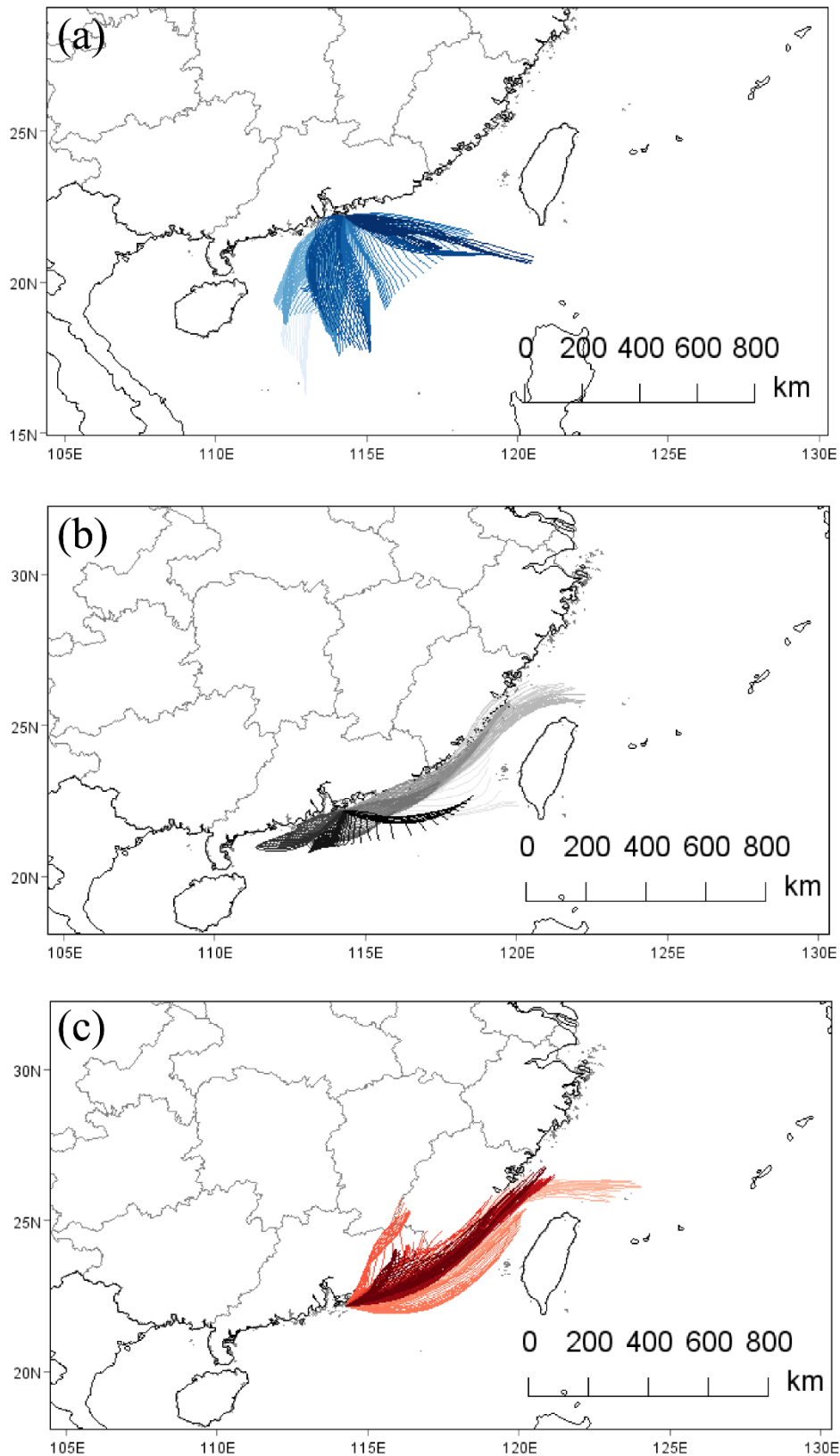
Figure S3. The 24-h backward trajectories of different kinds of air masses during the field campaign. The marine air masses occurred during 16–26 August and 11–23 September except 12, 15, and 16 September. The haze period occurred from 24 September to 2 October. The coastal air masses occurred during 4–31 October.

88

89
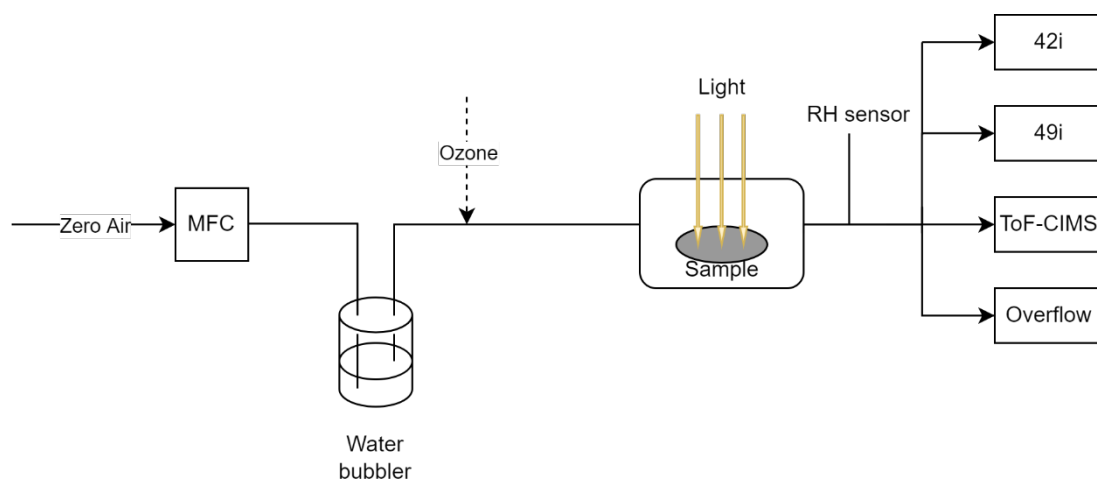
Figure S4. The schematic diagram of the photochemical aging experiment.

91

92
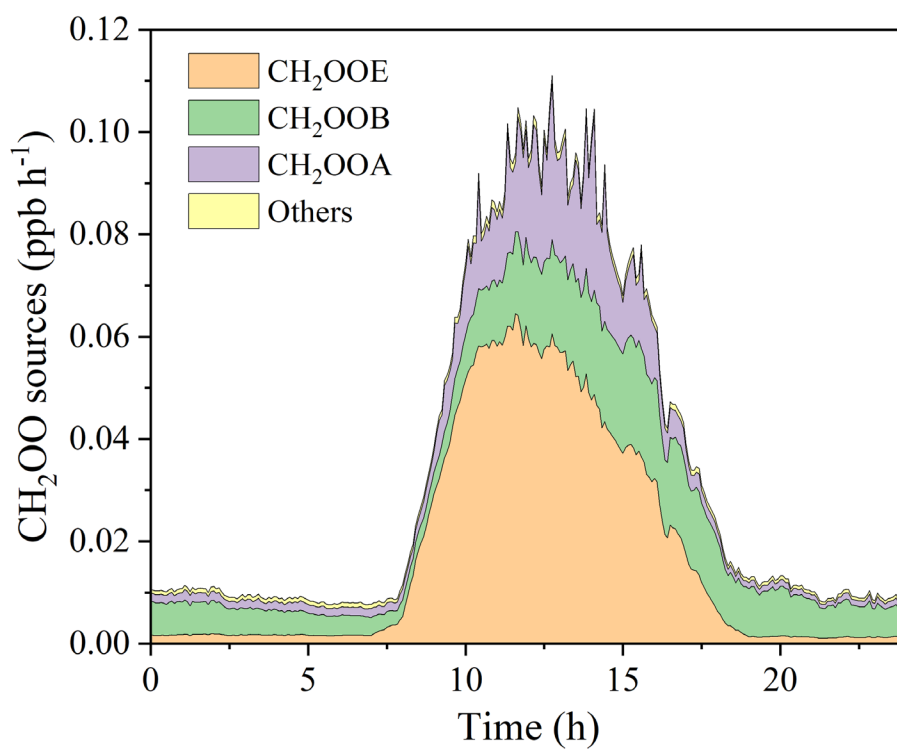
Figure S5. The sources of CH$_2$OO in the modified case on 28 September 2021.

94
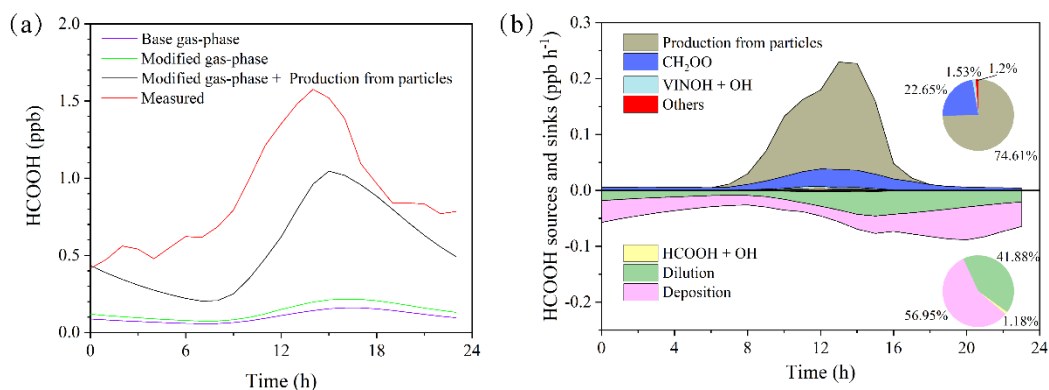
Figure S6. The model results on 28 October 2021. (a) The variations of HCOOH concentration. (b) The sources and sinks of HCOOH.
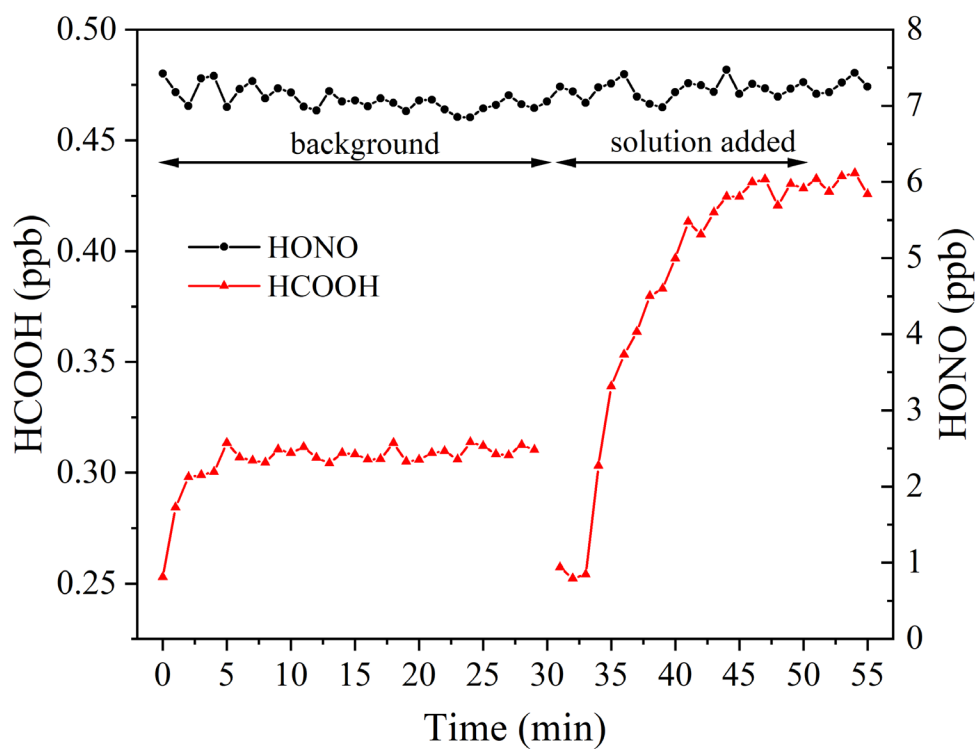
Figure S7. Additional laboratory experiments show that HCOOH was produced by nitrate rather than HONO.

Supplementary tables

Table S1. The instruments and measured species or parameters in the field campaign.

Species	Instruments	Time resolution
HCOOH, HONO, N_2O_5	Iodide-ToF-CIMS, Aerodyne Inc.	1 s
O_3	O_3 analyzer, model 49i, Thermo Scientific	1 min
NO, NO_2	NO_x analyzer, model 42i-TL with photolytic converter, Thermo Scientific	1 min
CO	CO analyzer, model T300U, Teledyne	1 min
SO_2	SO_2 analyzer, model T100U, Teledyne	1 min
jNO_2	Filter Radiometer, Metcon	1 min
VOCs	GC-MS/FID, Chromatotec Group	1 h
OVOCs	Carbonyl sampler, model 8000-2, ATEC HPLC	3 h
Particle number size distribution	Scanning mobility particle sizer, TSI	5 min
Compositions in $PM_{2.5}$ and PM_{10} (including Na^+, NH_4^+, K^+, Mg^{2+}, Ca^{2+}, Cl^-, NO_3^-, SO_4^{2-}	MARGA	1 h

Table S2. Summary of the $PM_{2.5}$ sampling information.

Date	RH	Size (cm^2)	Aerosol loading (mg)	Dry-state Surface area density
2020.10.07	72.34	51.6	3.33	192.52
2020.10.08	68.39	53.4	3.55	195.89
2020.10.26	78.85	53.4	4.28	119.86
2020.11.02	65.68	56.1	5.55	251.79

2020.11.03	69.82	52.51	4.40	233.81
2020.11.04	58.30	55.35	2.77	170.15
2020.11.05	76.32	53.352	1.95	134.89

106

107 **Table S3.** Input parameters to the box model of 28 September 2021.

Parameter	Diurnal average value	Parameter	Diurnal average value
Temp (K)	302.34 ± 1.47	M3PE	0.015 ± 0.01
RH(%)	78.84 ± 5.4	MEPROPENE	0.033 ± 0.005
jNO_2 (s^{-1})[1]	0.00744	BUT1ENE	0.011 ± 0.002
NO[2]	0.079 ± 0.082	ME2BUT1ENE	0.011 ± 0.003
NO2	1.82 ± 1.29	ME2BUT2ENE	0.005 ± 0.002
O3	57.28 ± 9.35	PENT1ENE	0.005 ± 0.001
CO	217.6 ± 11.3	APINENE	0.021 ± 0.008
SO2	4.99 ± 0.23	BPINENE	0.016 ± 0.006
N2O5	0.033 ± 0.025	EBENZ	0.012 ± 0.003
HONO	0.113 ± 0.026	OXYL	0.009 ± 0.001
CH4[3]	2000	M2PE	0.011 ± 0.012
C2H6	0.95 ± 0.11	HCHO	2.24 ± 0.28
C3H8	0.40 ± 0.11	CH3CHO	0.47 ± 0.11
IC4H10	0.40 ± 0.35	GLYOX	0.057 ± 0.024
NC4H10	0.17 ± 0.08	C2H5CHO	0.077 ± 0.012
IC5H12	0.27 ± 0.12	CH3COCH3	4.35 ± 3.54
NC5H12	0.09 ± 0.02	MGLYOX	0.076 ± 0.020
NC6H14	0.013 ± 0.008	MACR	0.013 ± 0.006
NC7H16	0.008 ± 0.004	IPRCHO	0.057 ± 0.003
NC8H18	0.006 ± 0.001	MEK	0.155 ± 0.013
C2H2	0.25 ± 0.03	BIACET	0.051 ± 0.005
C2H4	0.33 ± 0.05	C4H9CHO	0.016 ± 0.001
C3H6	0.04 ± 0.007	C5H11CHO	0.017 ± 0.002
C4H6	0.057 ± 0.004	BENZAL	0.012 ± 0.001
C5H8	0.82 ± 1.01	M23C4[3]	0.035
BENZENE	0.075 ± 0.014	M2HEX[3]	0.193
TOLUENE	0.11 ± 0.08	M3HEX[3]	0.158
MXYL	0.02 ± 0.008	TM123B[3]	0.029
M22C4	0.008 ± 0.001	TM124B[3]	0.018

108

109 [1] The data shown here is the highest value of jNO_2 (1-min resolution).

110   [2] The unit of the input data below is ppb.

111   [3] These air pollutants were assumed kept at a constant value.

112

113   **Reference**

114   Chu, L., & Anastasio, C. (2003). Quantum Yields of Hydroxyl Radical and Nitrogen

115   Dioxide from the Photolysis of Nitrate on Ice. *Journal of Physical Chemistry A*,

116   *107*(45), 9594–9602. https://doi.org/10.1021/jp0349132

117   Wolfe, G. M., Marvin, M. R., Roberts, S. J., Travis, K. R., & Liao, J. (2016). The

118   framework for 0-D atmospheric modeling (F0AM) v3.1. *Geoscientific Model*

119   *Development*, *9*(9), 3309–3319. https://doi.org/10.5194/GMD-9-3309-2016

120